DOI: 10.1002/ejic.201100391

Reactive and Organosoluble SnO_2 Nanoparticles by a Surfactant-Free Non-Hydrolytic Sol–Gel Route

Abdelhay Aboulaich,[a] Bruno Boury,*[a] and P. Hubert Mutin[a]

Keywords: Sol–gel processes / Nanoparticles / Nanostructures / Synthetic methods / Tin

Reactive SnO_2 nanoparticles have been successfully prepared by a simple non-hydrolytic sol–gel synthesis in CH_2Cl_2 at 110 °C by using $SnCl_4$ as a precursor and diisopropyl ether (iPr_2O) as an oxygen donor. The SnO_2 nanocrystals, with a diameter of about 4 nm, formed stable sols in organic aprotic solvents in the absence of any surfactant or coordinating agent. The lack of aggregation has been attributed to the presence of Cl and O*i*Pr surface groups instead of OH groups. These surface groups render the nanoparticles reactive towards hydroxylated surfaces, as shown by their reaction with an oxidized silicon wafer; the nanoparticles bind uniformly across the wafer to form a monolayer.

Introduction

Tin(IV) oxide is a semiconductor with a band gap of 3.6 eV at 300 K and has been investigated for potential applications as a sensor material,[1–5] photocatalyst,[6–8] anode material[9,10] as well as in photovoltaic devices.[11–13] Therefore there has been continuous interest in exploring synthetic routes to SnO_2 nanocrystals and nanostructures, including flame pyrolysis,[14,15] thermal evaporation,[4,16] laser ablation of massive SnO_2,[17] hydrothermal syntheses[18–22] and various sol–gel methods.[23–32]

Based on non-hydrolytic (or non-aqueous) sol–gel process,[33,34] Colvin et al. first reported on the synthesis of oxide and mixed-oxide nanoparticles.[35–37] The "benzyl alcohol" route based on the reaction of $SnCl_4$ [or Sn($OtBu)_4$] in benzyl alcohol appears particularly attractive for the synthesis of SnO_2-based nanocrystals[27,29,30,38,39] as it leads to well-crystallized nanoparticles that can be dispersed in organic solvents without the use of any additional stabilizers. Indeed, surfactants (e.g., trioctylphosphane oxide, oleic acid or octylamine) are commonly used in nanoparticle syntheses to prevent aggregation and control the size and sometimes the shape of the particles. However, the adsorbed surfactant may influence the toxicity of the nanoparticles and reduce accessibility to the nanoparticle surface as well as its reactivity, which could be detrimental to their applications in sensors or catalysis.[37] Therefore synthetic routes to oxide nanoparticles without any stabilizer are worth exploring.

We recently reported the synthesis, in the absence of any stabilizing agent, of easily dispersible silica, silica–titania and titania nanoparticles[40,41] using another non-hydrolytic sol–gel route (the "ether route"). Although the ether route has proved highly successful in the synthesis of mesoporous mixed-oxide catalysts,[42–44] it has not been used to prepare oxide nanoparticles.

This route is based on the reaction of silicon or metal chloride precursors with stoichiometric bis(isopropyl) ether (iPr_2O) as oxygen donor at moderate temperatures (80–150 °C). It involves in the first step the "etherolysis" of the chloride precursor leading to an isopropoxide [Equation (1)], which then condenses with the remaining chlorides [Equation (2)].[33,34]

$$[M]–Cl + iPr_2O \longrightarrow [M]–OiPr + iPr–Cl \quad (1)$$

$$[M]–O–iPr + Cl–[M] \longrightarrow [M–O–M] + iPr–Cl \quad (2)$$

In this paper we report the extension of the ether route to the synthesis of SnO_2 nanoparticles. Notably, we show that this route leads in very high yields to SnO_2 nanoparticles with several very original features: they can be redispersed in THF to form stable sols in the absence of any stabilizer, their surfaces appear to be terminated by residual Sn–Cl and Sn–O*i*Pr groups (instead of Sn–OH groups), which makes them highly reactive towards nucleophilic species, and they can react with hydroxylated Si wafers to form a monolayer of covalently bound nanoparticles.

Results and Discussion

The nanoparticles were obtained in one step by heating under autogenous pressure the precursor and oxygen donor diluted in CH_2Cl_2 [Equation (3)].

[a] Institut Charles Gerhardt de Montpellier, Chimie Moléculaire et Organisation du Solide, Université Montpellier 2, 34095 Montpellier, France
Fax: +33-4-67143852
E-mail: bruno.boury@univ-montp2.fr

Supporting information for this article is available on the WWW under http://dx.doi.org/10.1002/ejic.201100391.

$$SnCl_4 + 2\ i\mathrm{Pr}_2O \xrightarrow[60\ h,\ 110\ °C\ \text{Sealed tube}]{15\ \text{vol.}\ CH_2Cl_2} SnO_2 + 4\ i\mathrm{PrCl} \quad (3)$$

Information on the progress of the reaction was obtained by ^{1}H NMR analysis of the reaction mixture before and after heating at 110 °C (Figure 1; the sample prepared by heating at 110 °C is referred to as 110-SnO_2). The ^{1}H NMR spectrum recorded after heating shows the complete disappearance of the signals arising from iPr$_2$O (septuplet at δ = 3.69 ppm and doublet at δ = 1.15 ppm) and the presence of a septuplet at δ = 4.26 ppm and a doublet at δ = 1.55 ppm, which indicates the formation of a large amount (>95%) of the expected byproduct, iPrCl. A small signal at δ = 1.76 ppm (doublet of triplets) shows the presence of propylene, whereas the resonances at δ = 1.25 and $\delta \approx$ 0.9 ppm suggests the presence of propylene oligomers. These compounds likely arise from the thermal decomposition of iPrCl, leading to propylene and HCl, followed by the polymerization of propylene. Both reactions could be catalysed by Sn species. The yield (based on the weight of SnO_2 after calcination in air) was very high (88%).

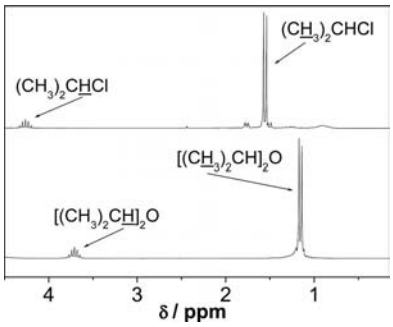

Figure 1. ^{1}H NMR spectra of the starting solution of mixed reagent before heating (bottom) and of the crude mixture after reaction at 110°C (top).

The TEM image of the 110-SnO_2 powder redispersed in THF evaporated on a grid (Figure 2) shows the presence of well-dispersed nanoparticles with rounded shapes; the nanoparticles exhibit a narrow size dispersity and an average diameter of about 4 nm. The absence of aggregation of the nanoparticles is ascribed to the chemistry involved in this process.[40,41] Indeed, in the absence of secondary reactions, the non-hydrolytic process used here leads to chloride and isopropoxide surface groups [Equations (2) and (3), Figure 3] instead of the Sn–OH groups usually present at the surface of oxide particles. The presence of residual Sn–Cl groups in the 110-SnO_2 sample (9.5 wt.-% Cl) was confirmed by the acid–base titration of an aqueous suspension of the powder, whereas the carbon content (8.9 wt.-%) is consistent with the presence of residual Sn–OiPr groups. The average formula derived from the C and Cl content is $SnO_{1.5}(OiPr)_{0.4}(Cl)_{0.6}$. This average formula is in good agreement with the weight loss (32%) determined by TGA in air for 110-SnO_2 (see Figure S1), assuming conversion to SnO_2.

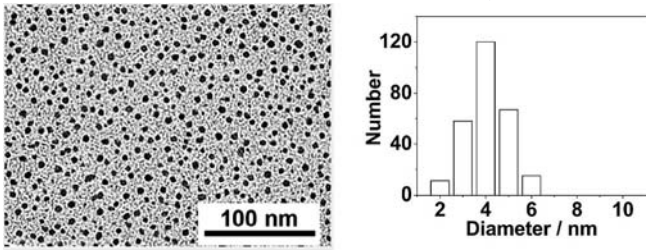

Figure 2. TEM image of the 110-SnO_2 nanoparticles after dispersion and dilution in THF (left) and the corresponding particle size distribution (right) determined by analysis of more than 200 particles.

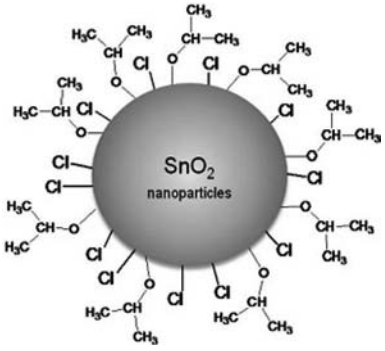

Figure 3. Schematic representation of a nanoparticle in 110-SnO_2.

At this point there is no control during the synthesis of the amount of residual chlorine and isopropoxide groups. As a stoichiometric amount of ether was used and as the etherolysis step appeared to be complete, the amount of residual chlorine and alkoxide groups should be similar. However, in principle it should be possible to favour the formation of either chloride or isopropoxide surface groups by using either an excess of $SnCl_4$ or an excess of iPr$_2$O. Another possibility would be a post-modification of the nanoparticles, for instance, with an alcohol, which would substitute the chloride and isopropoxide groups.

The absence of residual OH groups and the presence of OiPr were confirmed by FTIR spectroscopy (Figure 4). The bands characteristic of OiPr groups (C–H vibrations at 1364, 1455 and 2978 cm^{-1} and C–O vibrations at 1041 cm^{-1}) disappear upon calcination at 500 °C (sample denoted as 500-SnO_2). The 110-SnO_2 powder reacts readily with water and the spectrum of a sample exposed to ambient humidity is dominated by very broad bands at around 3000 cm^{-1} and a band at 1614 cm^{-1}, which indicate the presence of hydrogen-bonded OH groups and adsorbed water.

The dispersibility of the nanoparticles in aprotic organic solvents such as THF can be ascribed to the presence of surface Cl and OiPr groups, which make the nanoparticles organophilic. The stability of the sols (in the absence of water) has to be related to the very low rate of Cl/OiPr condensation [Equation (2)] at room temperature.

Conversely, the presence of Sn–Cl and Sn–OiPr functions and the absence of any stabilizing agent at the surface render these "naked" nanoparticles highly reactive towards

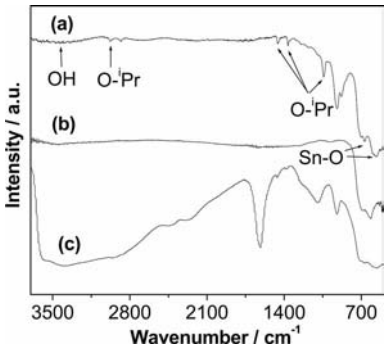

Figure 4. Transmission FTIR spectra of (a) dried 110-SnO_2, (b) 500-SnO_2 and (c) dried 110-SnO_2 nanoparticles after exposure to ambient humidity for 60 min.

nucleophiles such as water, alcohols or silanols. This reactivity allows SnO_2 nanoparticles to be anchored to hydroxylated surfaces, as depicted in Figure 5. The nanoparticles will bind to the surface by condensation of the surface hydroxy groups with residual Sn–Cl and Sn–O*i*Pr groups. Moreover, in the absence of water and at room temperature, the nanoparticles do not bind to each other by Sn–Cl/Sn–O*i*Pr condensation, thus the reaction should stop after the formation of a single monolayer of nanoparticles.

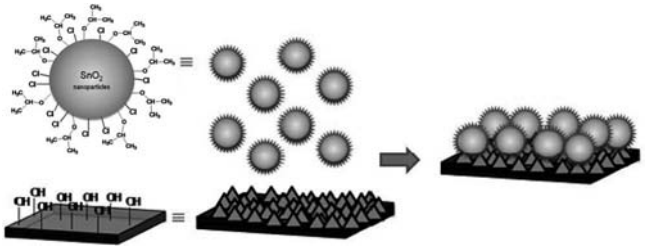

Figure 5. Deposition of a monolayer of SnO_2 nanoparticles by direct contact between reactive SnO_2 nanoparticles and an hydroxylated surface.

This was demonstrated by immersing an oxidized silicon wafer for 2 hours in a sol of 110-SnO_2 nanoparticles in THF (0.7 wt.-% in SnO_2). After washing the wafer in an ultrasonic bath an AFM image was recorded that shows the presence of a dense nanoparticle layer on the surface (Figure 6). The corresponding height distribution shows a sharp peak, ascribed to holes between nanoparticles, and a broader peak (shoulder) in the 3–8 nm range, consistent with the formation of a monolayer of nanoparticles.

Interestingly, the deposit can be tuned by changing the deposition solvent. Indeed, when the same procedure was performed in an ethanol/THF mixture (volume ratio 1:1), the number of particles anchored at the wafer surface drastically decreased (Figure 7). This indicates that the reactivity of the particles with the wafer surface decreased, most likely due to the reaction of the nanoparticles and/or wafer surface groups with EtOH. However, the height of the particles dispersed on the wafer surface ranged between 5 and 8 nm, which suggests some aggregation of the nanoparticles, possibly due to the presence of traces of water in the ethanol used.

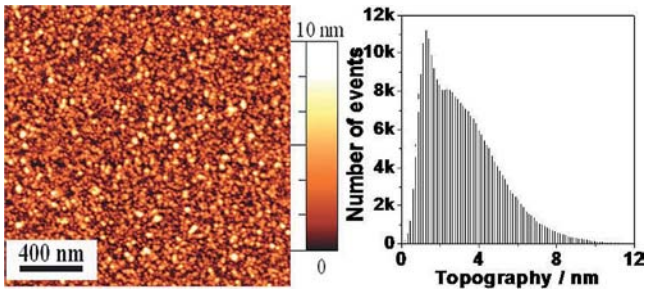

Figure 6. AFM image of a monolayer of 110-SnO_2 nanoparticles deposited on an oxidized Si wafer (left) and the corresponding height distribution (right).

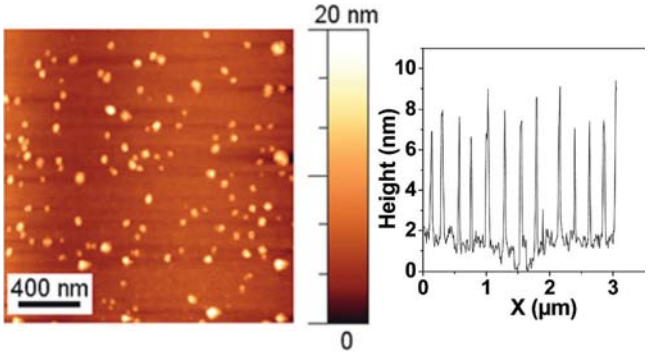

Figure 7. AFM image of the surface of a silicon wafer after dipping for 2 h in a CH_2Cl_2/EtOH/110-SnO_2 sol (left) and corresponding height profile (right) across the surface.

The powder XRD pattern of dried 110-SnO_2 (Figure 8) shows the presence of poorly crystalline SnO_2. The particularly broad reflection at around 27° suggests the presence of an amorphous phase, possibly adsorbed organic compounds. This broad component disappears after treatment in air at 300 °C (300-SnO_2), whereas the other reflections were not significantly affected. As expected, heat treatment at 400 (400-SnO_2) and 500 °C (500-SnO_2) led to the growth of SnO_2 crystals, as shown by the decrease of the peak widths. All the peaks could be indexed to the standard cassiterite SnO_2 phase (JCPDS Card No. 41-1445). The average crystallite size [estimated from the widths of the (110) and (101) reflections using Scherrer's equation] increases from about 3 to 14 nm (Table 1) between 300 and 500 °C.

The growth of the SnO_2 crystallites is also evidenced by the decrease in the specific surface area from 180 $m^2 g^{-1}$ for dried 110-SnO_2 to 70 $m^2 g^{-1}$ for 500-SnO_2 (Table 1). The average diameters estimated from the specific surface areas are similar to those determined from the XRD patterns, which indicates that the nanoparticles are monocrystalline and non-porous.

The TEM images (Figure 9) of dried 110-SnO_2 show the presence of small spherical aggregates of around 15 nm built of primary nanoparticles (≈4 nm). After calcination at 500 °C, spherical aggregates with diameters of around 300 nm formed by the self-assembly of primary nanoparticles (≈15 nm). A similar morphology has previously been

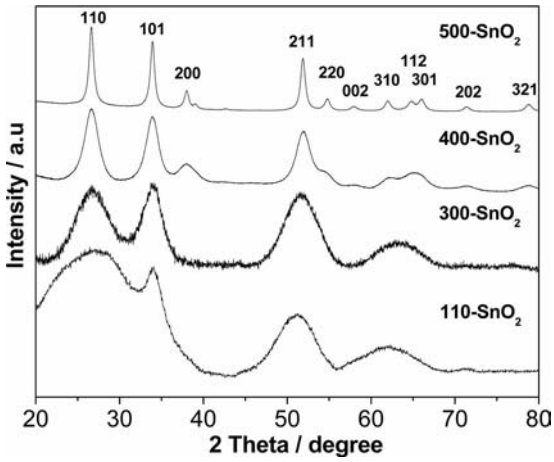

Figure 8. XRD patterns of dried 110-SnO_2 before and after calcination for 2 h at 300, 400 and 500 °C in dry air.

Table 1. Average diameters of the nanoparticles estimated by porosimetry (BET method) and XRD.

Samples	BET S [$m^2 g^{-1}$], D [nm][a]	XRD D [nm]
Dried 110-SnO_2	180, 4.8	–
300-SnO_2	180, 4.8	3.1
400-SnO_2	90, 9.7	8.4
500-SnO_2	70, 12.4	13.9

[a] Calculated from the specific surface area S by using the expression $D = 6000/(dS)$, with d representing the cassiterite density (6.9).

reported for mesoporous titania–vanadia catalysts prepared by the same non-hydrolytic sol–gel route.[42]

The Raman spectra of the different samples are displayed in Figure 10. All the spectra show the A_{1g} (630 cm^{-1}) and B_{2g} (770 cm^{-1}) modes typical of the tetragonal structure of cassiterite. In addition, the spectra of 110-SnO_2, 300-SnO_2 and 400-SnO_2 display a very broad feature between 400 and 700 cm^{-1} and several bands in the 200–400 cm^{-1} region. These 200–400 cm^{-1} bands have previously been reported for several nanostructured SnO_2, but their origin has not yet been elucidated.[45] The very broad feature between 400 and 700 cm^{-1} has been ascribed to surface modes and is very sensitive to the specific surface area and the level of crystallinity of the particles.[46]

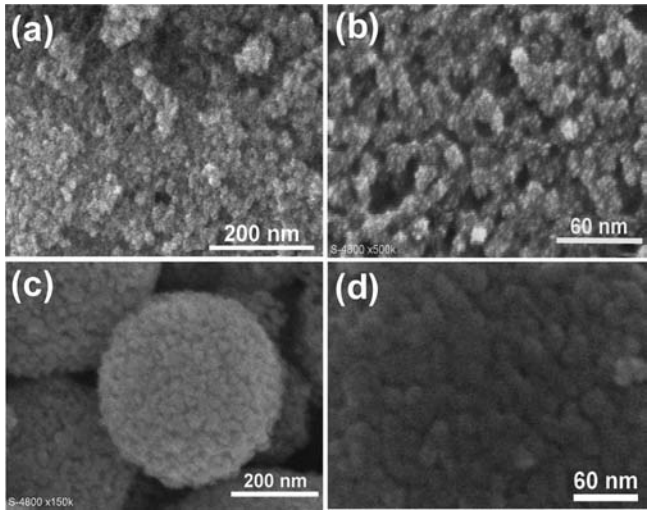

Figure 9. SEM images of (a,b) dried 110-SnO_2 and (c,d) 500-SnO_2.

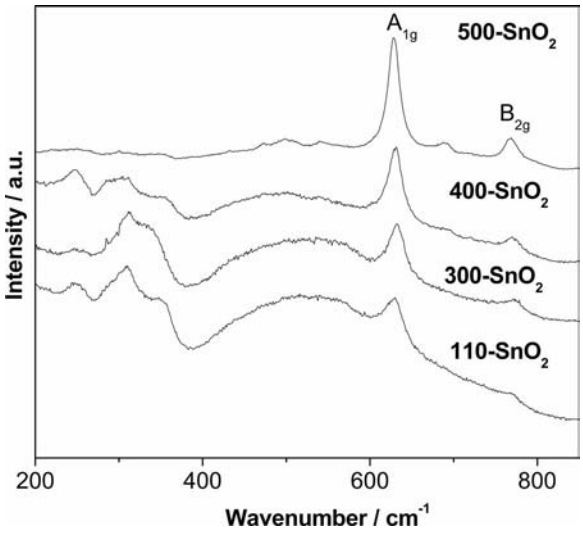

Figure 10. Raman spectra of the SnO_2 samples.

Indeed, in our case, the intensity of this band decreased with the specific area. Interestingly, a clear correlation has been reported between the intensity of the surface modes and the response of SnO_2 gas sensors to CO.[45]

Conclusions

The results reported herein show that organo-soluble and reactive SnO_2 nanoparticles with low size polydispersity can be obtained by the reaction of $SnCl_4$ with a stoichiometric amount of $i$$Pr_2O$ in CH_2Cl_2 at 110 °C. The nanoparticles can be easily dispersed in THF, leading to a stable sol of well-dispersed nanoparticles (≈4 nm). These nanoparticles appear to be terminated by chloro and isopropoxy groups, which accounts for their original properties: their organophilic character, the absence of aggregation at room temperature in the absence of water and their reactivity towards nucleophiles. This unique surface chemistry and the absence of non-hydrolytic condensation at room temperature allow the self-limiting anchoring of nanoparticles to hydroxylated surfaces. The low synthesis temperature, the excellent yield and the high surface area of the nanoparticles are additional valuable points. This simple synthetic route should be applicable to other metal oxides, provided that the chloride precursors are soluble in aprotic organic solvents such as dichloromethane or chloroform.

Experimental Section

Materials: Tin tetrachloride (99.99% Aldrich) was used without further purification. Bis(isopropyl) ether ($i$$Pr_2O$; 99% Acros) and tetrahydrofuran (THF; 99% VWR) were purified by distillation over sodium wire under N_2 and CH_2Cl_2 by distillation over P_2O_5.

Synthesis of SnO_2 Nanoparticles: All manipulations were carried out under argon using standard Schlenk techniques and a glovebox (MBRAUN, $H_2O < 0.1$ ppm, $O_2 < 0.1$ ppm). The water content in $i Pr_2O$ and CH_2Cl_2 (determined by Karl-Fischer titration) was lower than 10 ppm. In a typical experiment, $SnCl_4$ (1.33 g, 5.11 mmol), iPr_2O (1.045 g, 10.22 mmol) and CH_2Cl_2 (31 mL) were successively introduced under argon into a 70 mL Pyrex tube that was sealed after freezing the mixture in liquid nitrogen. The tube was heated at 110 °C for 60 h, then cooled to room temperature and opened in a glovebox. The white suspension was transferred to a centrifugation tube, which was closed, and the precipitate isolated by centrifugation (10 min, 20000 rpm). The white precipitate (110-SnO_2) was redispersed in THF and stored in a glovebox. For characterization purposes, 110-SnO_2 was dried under vacuum at room temperature for 3 h prior to measurements. The resulting powder is referred to as "dried 110-SnO_2". Samples of dried 110-SnO_2 were further calcined in air for 2 h at 300, 400 and 500 °C.

Grafting of SnO_2 Nanoparticles onto Silicon Wafers: A silicon wafer (dimensions 1×2 cm) was first washed with CH_2Cl_2 (previously filtered through a 0.45 μm filter) in an ultrasonic bath and then treated for 1 h in a home-made UV/O_3 reactor to obtain an hydroxylated silica surface. The nanoparticles were deposited by dipping the wafer into 110-SnO_2 nanoparticles dispersed in THF for 2 h at 25 °C under argon. The wafer was then washed three times with CH_2Cl_2 and dried in a glovebox.

Characterization: Transmission electron microscopy (TEM) was performed with a JEOL 1200 EXII instrument operated at 100 kV. The samples were prepared by adding one drop of a diluted SnO_2/THF sol on to a Cu grid. Atomic force microscopy (AFM) images of the nanoparticles deposited on a Si wafer were obtained in tapping mode with a Dimension 3100 instrument equipped with a Nanoscope IIIA controller from Veeco Instruments. Scanning electron microscopy (SEM) images were obtained with an Hitachi S-4500 microscope operated at 30 kV. ^1H NMR spectra were obtained with a Bruker Avance 200 spectrometer. Infrared spectra were recorded with a Thermo Nicolet Avatar 320 FTIR spectrophotometer scanning from 500 to 3500 cm^{-1} with a resolution of 4 cm^{-1} for 32 scans. The samples were placed between two NaCl plates. Raman spectra were obtained with a Jobin–Yvon LabRAM ARAMIS spectrometer equipped with an ×50 objective and CCD detector. The samples were irradiated at 473 nm. X-ray diffraction experiments were performed with a Philips X′pert Pro MPD diffractometer used in θ/θ mode with λ(Cu-$K_{\alpha 1}$) = 1.5406 Å. N_2 physisorption experiments were performed at 77 K with a Micromeritics ASAP 2010 sorptometer. The samples were previously degassed under vacuum at 120 °C for 15 h. The specific surface areas of the powders were calculated by using the BET method, assuming an area of 0.162 nm^2 per N_2 molecule. Thermogravimetric analysis was performed under dry air from room temperature to 800 °C at a heating rate of 10 °C min^{-1} on a Netzsch STA 409 PC Luxx apparatus. The carbon and hydrolysable chlorine contents were measured on the dried powders by combustion and acid–base titration of an aqueous suspension, respectively.

Supporting Information (see footnote on the first page of this article): Thermogravimetric analysis of dried 110-SnO_2 nanoparticles.

Acknowledgments

We wish to thank Prof. Thierry Toupance from ISM Bordeaux 1 for fruitful discussions on the synthesis and characterization of the SnO_2 nanoparticles.

[1] P. G. Harrison, M. J. Willett, *Nature* **1988**, *332*, 337.
[2] M. Law, H. Kind, B. Messer, F. Kim, P. Yang, *Angew. Chem.* **2002**, *114*, 2511; *Angew. Chem. Int. Ed.* **2002**, *41*, 2405.
[3] G.-J. Li, X.-H. Zhang, S. Kawi, *Sens. Actuators B* **1999**, *60*, 64.
[4] B. Wang, L. F. Zhu, Y. H. Yang, N. S. Xu, G. W. Yang, *J. Phys. Chem. C* **2008**, *112*, 6643.
[5] G. X. Wang, J. S. Park, M. S. Park, X. L. Gou, *Sens. Actuators B* **2008**, *131*, 313.
[6] F. Fresno, M. D. Hernandez-Alonso, D. Tudela, J. M. Coronado, J. Soria, *Appl. Catal. B* **2008**, *84*, 598.
[7] D. Robert, *Catal. Today* **2007**, *122*, 20.
[8] K. Vinodgopal, I. Bedja, V. K. Prashant, *Chem. Mater.* **1996**, *8*, 2180.
[9] F. Cheng, Z. Tao, J. Liang, J. Chen, *Chem. Mater.* **2008**, *20*, 667.
[10] N. Zhao, L. Fu, L. Yang, T. Zhang, G. Wang, Y. Wu, T. v. Ree, *Pure Appl. Chem.* **2008**, *80*, 2283.
[11] A. Shah, P. Torres, R. Tscharner, N. Wyrsch, H. Keppner, *Science* **1999**, *285*, 692.
[12] H. Imahori, *J. Mater. Chem.* **2007**, *17*, 31.
[13] A. Kay, M. Graetzel, *Chem. Mater.* **2002**, *14*, 2930.
[14] W. H. Zhu, S. E. Pratsinis, *AIChE J.* **1997**, *43*, 2657.
[15] T. Sahm, L. Madler, A. Gurlo, N. Barsan, S. E. Pratsinis, U. Weimar, *Sens. Actuators B* **2004**, *98*, 148.
[16] M. S. Park, G. X. Wang, Y. M. Kang, D. Wexler, S. X. Dou, H. K. Liu, *Angew. Chem.* **2007**, *119*, 764; *Angew. Chem. Int. Ed.* **2007**, *46*, 750.
[17] J. Q. Hu, Y. Bando, Q. L. Liu, D. Golberg, *Adv. Funct. Mater.* **2003**, *13*, 493.
[18] B. Cheng, J. M. Russell, W. S. Shi, L. Zhang, E. T. Samulski, *J. Am. Chem. Soc.* **2004**, *126*, 5972.
[19] A. A. Firooz, A. R. Mahjoub, A. A. Khodadadi, *Mater. Lett.* **2008**, *62*, 1789.
[20] X. W. Lou, Y. Wang, C. Yuan, J. Y. Lee, L. A. Archer, *Adv. Mater.* **2006**, *18*, 2325.
[21] H. X. Yang, J. F. Qian, Z. X. Chen, X. P. Ai, Y. L. Cao, *J. Phys. Chem. C* **2007**, *111*, 14067.
[22] G. Xi, Y. He, Q. Zhang, H. Xiao, X. Wang, C. Wang, *J. Phys. Chem. C* **2008**, *112*, 11645.
[23] V. Briois, S. Belin, C. M. Zucolotto, R. H. A. Santos, C. V. Santilli, S. H. Pulcinelli, *Chem. Mater.* **2004**, *16*, 3885.
[24] T. F. Baumann, S. O. Kucheyev, A. E. Gash, J. H. Satcher Jr., *Adv. Mater.* **2005**, *17*, 1546.
[25] L. Renard, H. Elhamzaoui, B. Jousseaume, T. Toupance, G. Laurent, F. Ribot, H. Saadaoui, J. Broetz, H. Fuess, R. Riedel, A. Gurlo, *Chem. Commun.* **2011**, *47*, 1464.
[26] T. Toupance, O. Babot, B. Jousseaume, G. Vilaca, *Chem. Mater.* **2003**, *15*, 4691.
[27] T. G. Conti, A. J. Chiquito, R. O. da Silva, E. Longo, E. R. Leite, *J. Am. Ceram. Soc.* **2010**, *93*, 3862.
[28] J. H. Harreld, J. Sakamoto, B. Dunn, *J. Power Sources* **2003**, *115*, 19.
[29] V. Muller, M. Rasp, G. Stefanic, J. Ba, S. Gunther, J. Rathousky, M. Niederberger, D. Fattakhova-Rohlfing, *Chem. Mater.* **2009**, *21*, 5229.
[30] J. Ba, J. Polleux, M. Antonietti, M. Niederberger, *Adv. Mater.* **2005**, *17*, 2509.
[31] T. Kida, T. Doi, K. Shimanoe, *Chem. Mater.* **2010**, *22*, 2662.
[32] S. de Monredon, A. Cellot, F. Ribot, C. Sanchez, L. Armelao, L. Gueneau, L. Delattre, *J. Mater. Chem.* **2002**, *12*, 2396.
[33] A. Vioux, *Chem. Mater.* **1997**, *9*, 2292.
[34] P. H. Mutin, A. Vioux, *Chem. Mater.* **2009**, *21*, 582.
[35] T. J. Trentler, T. E. Denler, J. F. Bertone, A. Agrawal, V. L. Colvin, *J. Am. Chem. Soc.* **1999**, *121*, 1613.
[36] J. Joo, T. Yu, Y. W. Kim, H. M. Park, F. Wu, J. Z. Zhang, T. Hyeon, *J. Am. Chem. Soc.* **2003**, *125*, 6553.
[37] M. Niederberger, *Acc. Chem. Res.* **2007**, *40*, 793.
[38] J. Ba, D. F. Rohlfing, A. Feldhoff, T. Brezesinski, I. Djerdj, M. Wark, M. Niederberger, *Chem. Mater.* **2006**, *18*, 2848.

[39] G. Neri, A. Bonavita, G. Micali, G. Rizzo, N. Pinna, M. Niederberger, J. Ba, *Sens. Actuators B* **2008**, *130*, 222.
[40] A. Aboulaich, O. Lorret, B. Boury, P. H. Mutin, *Chem. Mater.* **2009**, *21*, 2577.
[41] A. Aboulaich, B. Boury, P. H. Mutin, *Chem. Mater.* **2010**, *22*, 4519.
[42] D. P. Debecker, K. Bouchmella, R. Delaigle, P. Eloy, C. Poleunis, P. Bertrand, E. M. Gaigneaux, P. H. Mutin, *Appl. Catal. B* **2010**, *94*, 38.
[43] A. M. Cojocariu, P. H. Mutin, E. Dumitriu, F. Fajula, A. Vioux, V. Hulea, *Appl. Catal. B* **2010**, *97*, 407.
[44] D. P. Debecker, K. Bouchmella, C. Poleunis, P. Eloy, P. Bertrand, E. M. Gaigneaux, P. H. Mutin, *Chem. Mater.* **2009**, *21*, 2817.
[45] M. N. Rumyantseva, A. M. Gaskov, N. Rosman, T. Pagnier, J. R. Morante, *Chem. Mater.* **2005**, *17*, 893.
[46] A. Dieguez, A. Romano-Rodriguez, A. Vila, J. R. Morante, *J. Appl. Phys.* **2001**, *90*, 1550.

Received: April 11, 2011
Published Online: July 19, 2011

